

Electronic Supporting Information - Ion Shuttling between Emulsion Droplets by Crown Ether Modified Gold Nanoparticles

Contents

1. Emulsions	1
2. Representative Optical Microscopy Images of Different Emulsion Droplets	3
3. Cation/Anion Effects	7
4. Complexation of Cations within the Emulsion Droplets	8
5. GNP Phase Transfer	16
6. Cryo-SEM.....	17
7. Movie of BaSO ₄ Precipitation	18
References.....	19

1. Emulsions

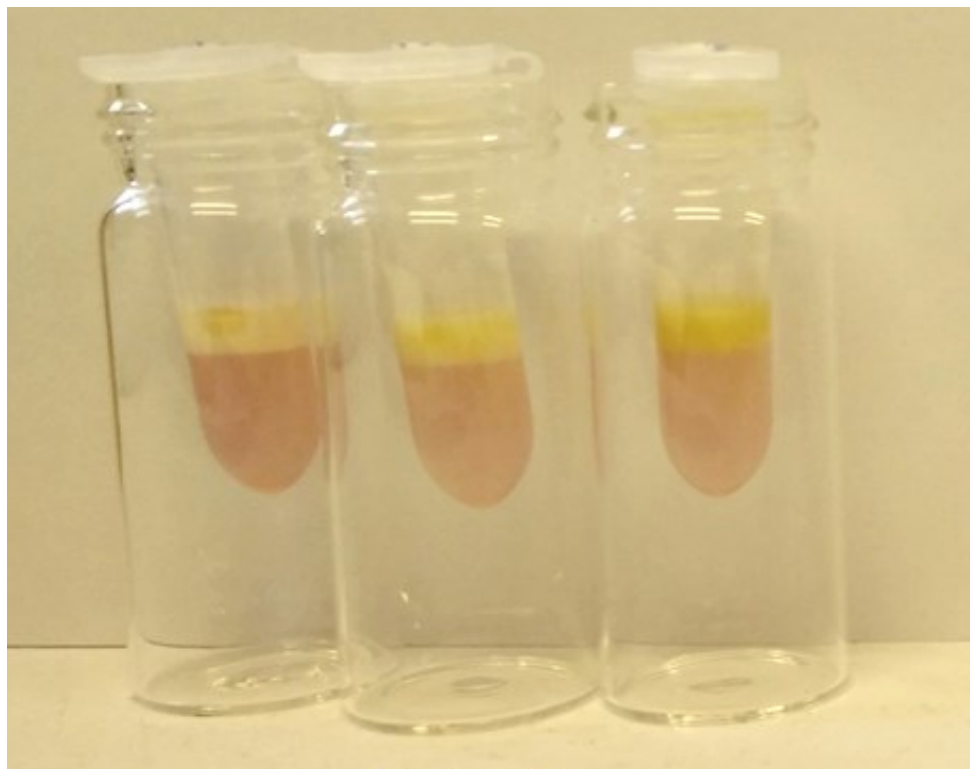


Figure ESI1: Freshly prepared water-in-chloroform emulsions. The emulsions are the opaque yellow layers on top of the clear red continuous phase (chloroform). The dominant yellow colour of the

emulsions is due to the presence of the fluorescent dye calcein. The red colour of the chloroform stems from the partitioning GNPs.

Based on literature methods^[1], stable water-in-oil emulsions were obtained with *Span80* as a surfactant with the optimal hydrophilic-lipophilic balance (HLB).^[2] A number of different oil phases were tested. Decane^[3] (Figure ESI6) and toluene (Figure ESI7) led to stable emulsions but no GNP mediated transport between the droplets could be observed. Chloroform both supported transport by GNPs, and gave very stable emulsions (Figure ESI2). Droplet size distributions were measured five minutes after mixing, and again after four days. There was no significant change. The ability of chloroform to support GNP phase transfer is believed to be linked to its relatively high polarity. These findings indicate that *direct transfer* between adjacent droplets is also dependent on the ability of the particles to partition between the two solvents. While surfactant mediated transport of fluorescent molecules and ions are recognised phenomena in some emulsions,^[4-5] we found no evidence of this in our experiments. In the absence of GNPs, no partitioning of the calcein dye between the droplets was observed, and no precipitation of BaSO₄ occurred.

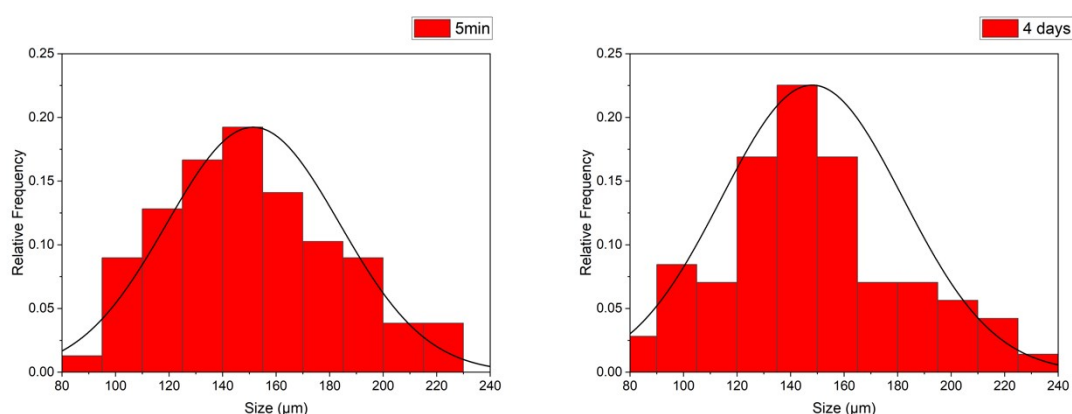


Figure ESI2 Size distribution of droplets obtained via ImageJ, counting around 100 droplets 5 minutes after mixture (left) and again after 4 days (right). Mean diameter is 151.4 µm (± 32 µm) and 148.1 µm (± 33 µm), respectively.

2. Representative Optical Microscopy Images of Different Emulsion Droplets

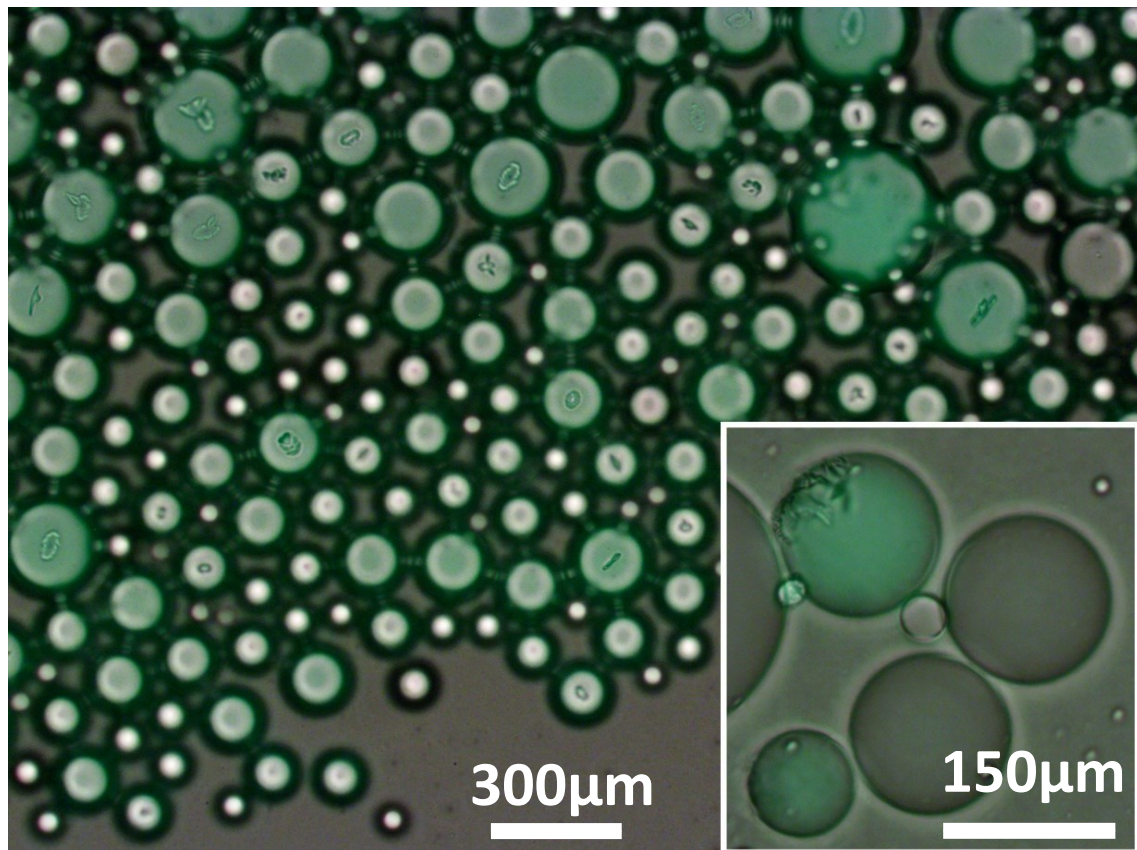


Figure ES13 Emulsion mixture clearly showing precipitate in the calcein stained droplet (green fluorescent). At 20x magnification, with insert showing precipitate growing on the interface (40x magnification). Note: At low magnification and with small droplets the green fluorescent light reflects on the droplet interfaces and makes all droplets appear green.

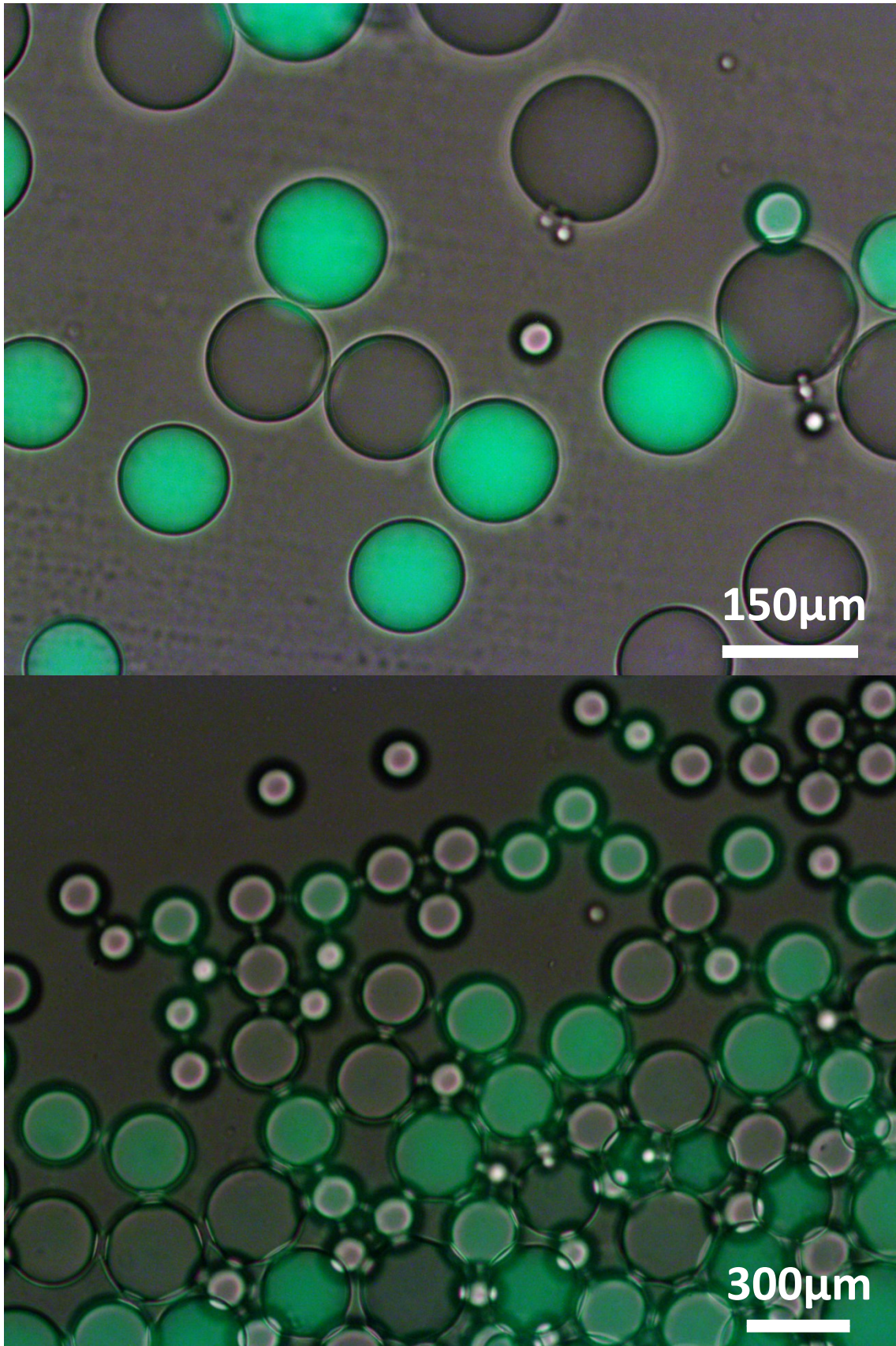


Figure ESI4 Emulsion mixtures with no GNP transporter present yields no precipitate (40x magnification top and 20x, bottom)

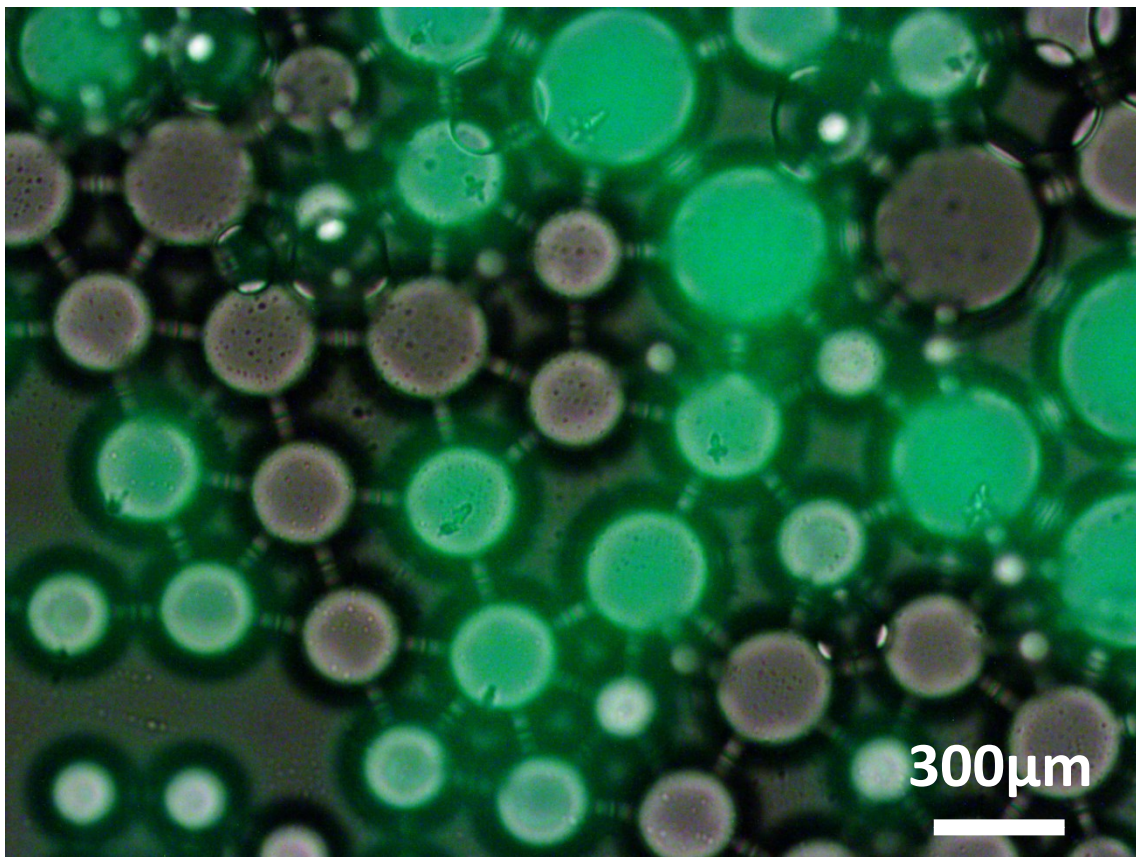
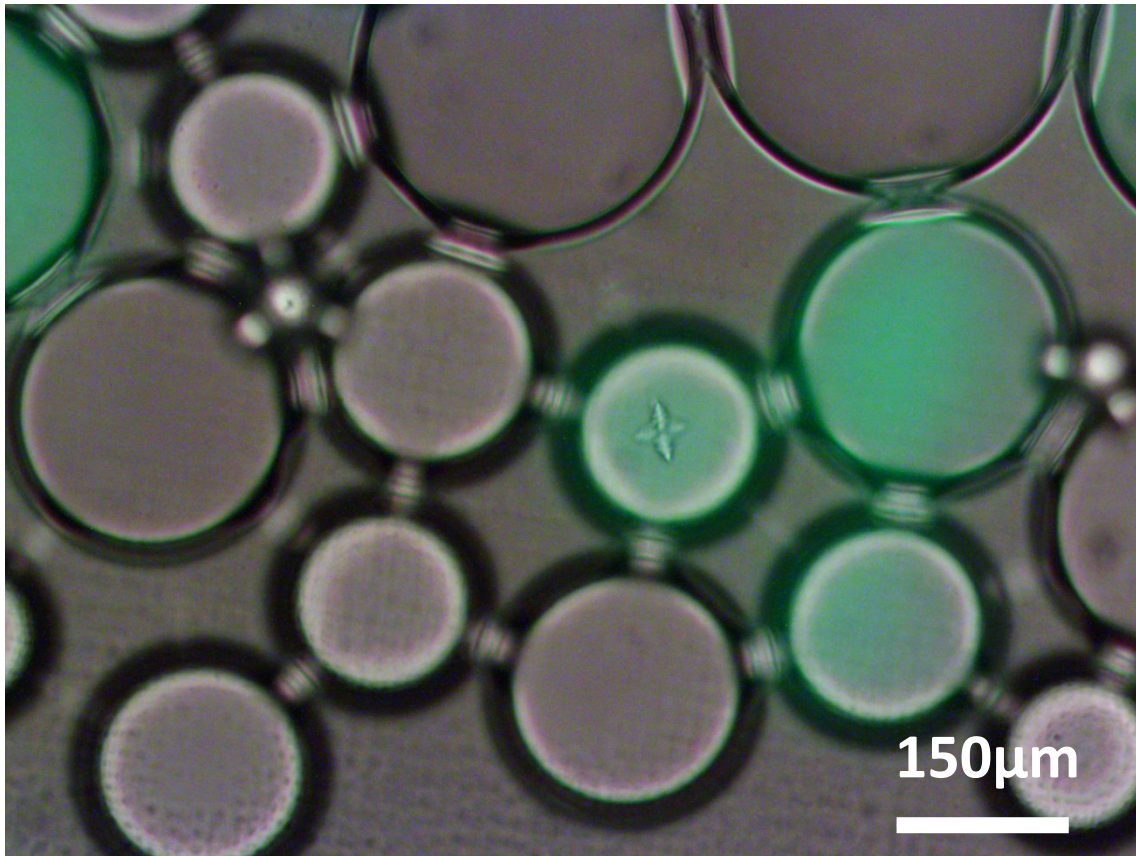


Figure ES15 Emulsion mixture (sample 2) with GNP transporter and Fe(II) present in the target droplet, yielding large amount of BaSO₄ precipitate (40x magnification top and 20x, bottom).

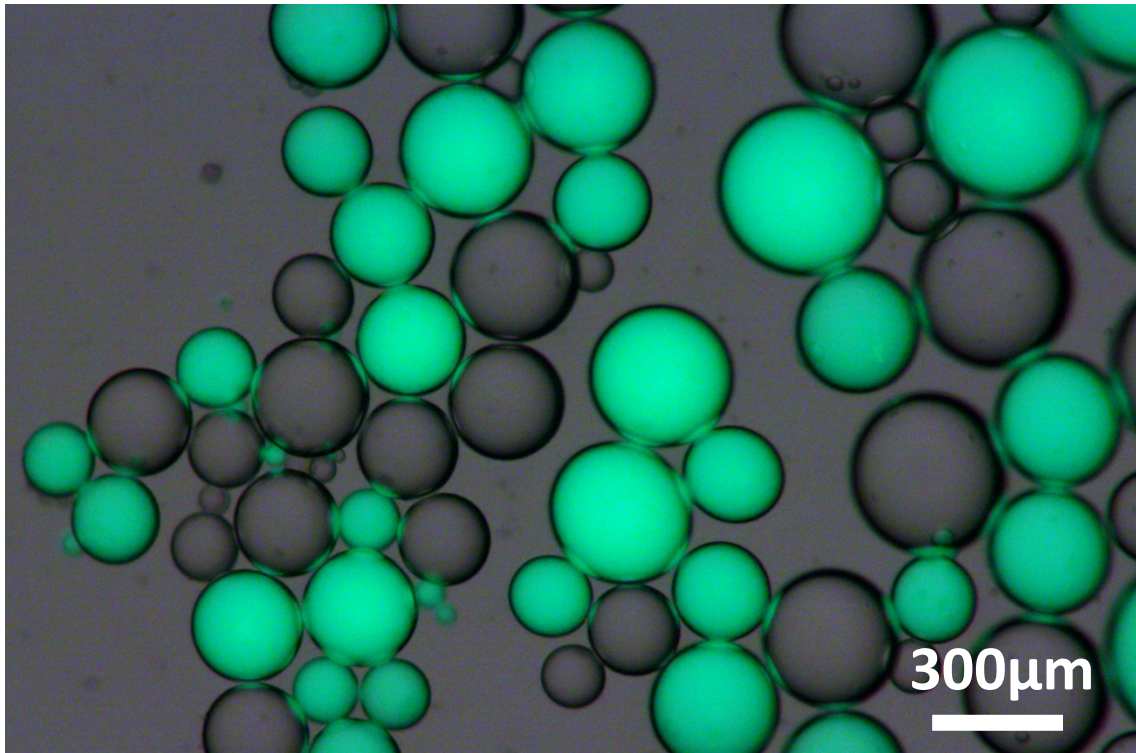


Figure ESI6 Decane based emulsion mixture with GNP transporter, after 4 days (20x magnification).

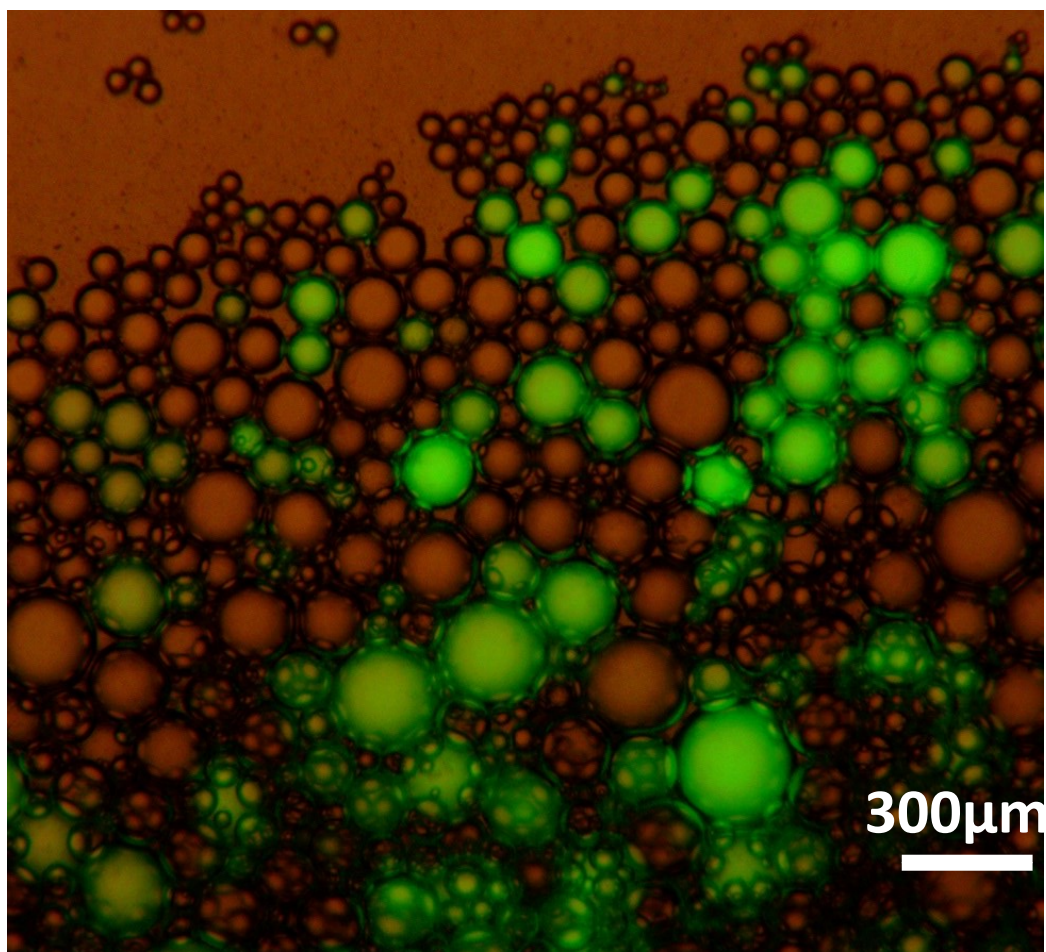


Figure ESI7 Toluene based emulsion mixture with GNP transporter, after 1 day (20x magnification).

3. Cation/Anion Effects

Screening for potential anion and/or cation effects was carried out using a range of different salts as sources for both barium and for sulfate. The experiments were conducted following the same procedure outlined in the manuscript, where two emulsions solutions were prepared, one containing the barium *source* along with the GNP transporters and the other containing the sulfate *target*. By manually counting the precipitate crystals observed in the micrographs, the efficiency of the alternative sources was estimated. Figure ESI8 shows the results for $\text{Ba}(\text{ClO}_4)_2$, $\text{Ba}(\text{C}_2\text{H}_3\text{O}_2)_2$ and $\text{Ba}(\text{NO}_3)_2$. All were used as 25 mM solutions as with BaCl_2 (shown for comparison).

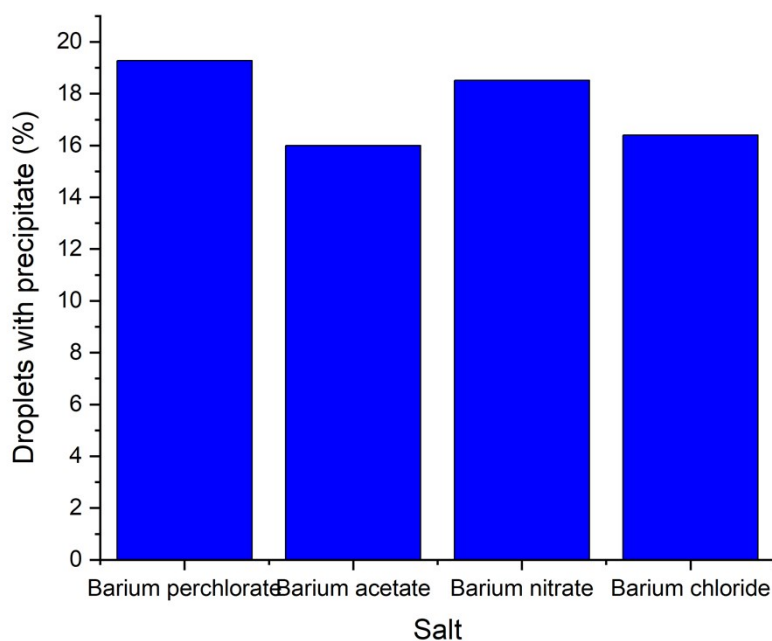


Figure ES18 Addition of various sources of barium, yielding comparable results for precipitation.

Figure ES19 shows the results for alternative sulfates, namely Cs_2SO_4 , MgSO_4 and Li_2SO_4 (also used in 25 mM). A typical value for K_2SO_4 is also shown for comparison. The choice of cation appears to have little to no influence on the amount of precipitate formed.

Note that higher concentrations of GNPs were used here, compared to the values presented in Figure ES18 and in Table 1 in the paper. Direct quantitative comparison of all data presented is therefore not possible.

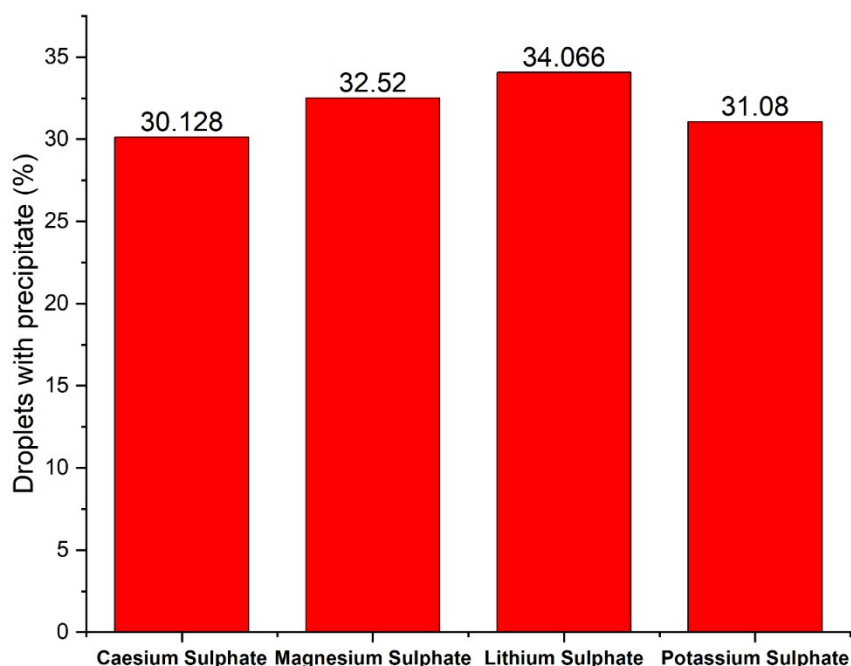


Figure ES19 Addition of various sources of sulfate yielding comparable amounts of precipitates. Note: higher concentration of GNP used here compared to the values presented in ES18 and Table 1.

4. Complexation of Cations within the Emulsion Droplets

Complexation of *18-crown-6* ligands with group I and group II cations has been widely investigated^[6,7] consistently showing first-order complex formation kinetics (Table ES11) and reversible zero-order dissociation with characteristic fast reactions times for both direct and inversed reactions. Similarly, thermodynamic complexation data in water for *18-crown-6* ligands have been determined for a wide range of structural variations showing only small effects on the equilibrium constants for Ba^{2+} and K^+ , suggesting that the coordination centre of *18-crown-6* ligands is not significantly affected by non-coordinating substituent groups in the macrocycle.^[7] The fast kinetics and robust thermodynamic behaviour of this ligand will allow us to apply in the following sections a quasi-equilibrium approximation within each emulsion droplet, assuming that the dynamics of formation and dissociation of metal complexes are much faster than the diffusion of shuttle GNPs between the droplets and that the coordination properties of the ligand are not significantly affected within the micro-heterogeneous system.

Table ESI1 Thermodynamic equilibrium constants (K^{eq}), kinetic constants of formation (k^f) and dissociation (k^d) for metal complexes in water. (Data obtained from reference⁵.)

	Equilibrium constant	Kinetic rate constants	
cation	$\log K_{M:crown}^{eq}$	$k_{M:crown}^f (M^{-1} s^{-1})$	$k_{M:crown}^d (s^{-1})$
Ba ²⁺	3.87	$1.3 \cdot 10^8$	$1.7 \cdot 10^4$
K ⁺	2.03	$4.3 \cdot 10^8$	$3.7 \cdot 10^6$
Cs ⁺	0.98	$7.8 \cdot 10^9$	$4.4 \cdot 10^7$
Na ⁺	0.80	$2.2 \cdot 10^8$	$7.9 \cdot 10^7$
Ca ²⁺	0.48	$< 1 \cdot 10^8$	$> 3.2 \cdot 10^7$
Li ⁺	≈ 0	$\approx 8 \cdot 10^7$	$\approx 6 \cdot 10^7$

Complexation Equilibrium within Source Droplets.

The source droplets contain BaCl₂ ($[Ba^{2+}]_0 = 25mM$) and crown-ether ligands anchored to the GNPs (initial ligand concentration 5 μ M, based on GNP concentration and estimated ligand coverage). Under equilibrium conditions, the concentrations of free cation [Ba²⁺], free ligand [crown] and complex [crown:Ba²⁺] obey the law of mass action equation:

$$K_{crown:Ba^{2+}}^{eq} = \frac{[crown:Ba^{2+}]}{[Ba^{2+}] \cdot [crown]}$$

Where $K_{crown:Ba^{2+}}^{eq}$ is the apparent complexation constant. Using this expression and the data in Table ESI1, we can estimate the initial ratio of complex to free ligand within the source emulsion:

$$\frac{[crown:Ba^{2+}]}{[crown]} = [Ba^{2+}]_0 \cdot K_{crown:Ba^{2+}}^{eq} = 143.8$$

The value obtained suggests that under starting conditions of the source emulsion, barium complexation is considerably favoured, with over 99% of the ligand molecules coordinated to Ba²⁺ ions. Interestingly, when Ba²⁺ is being transported out by the shuttle NPs, a reduction of one order of magnitude on the concentration of Ba²⁺ would lead only to a slight decrease of the complexation extent within the source emulsion (95% of complexation for 2.5mM of Ba²⁺), evidencing the strong affinity of the ligand for Ba²⁺.

Complexation Equilibrium within Target Droplets

We follow a similar approach to describe the complexation equilibria in the target droplets, but considering in this case also the precipitation equilibrium of BaSO₄. As the shuttle GNPs diffuse from the source droplet to the target droplet, they carry complexed Ba²⁺, which can subsequently react with SO₄²⁻ present in the target droplets. The processes involved here can be associated to the equilibrium constants as follow:

$$K_{crown:Ba^{2+}}^{eq} = \frac{[crown:Ba^{2+}]}{[Ba^{2+}] \cdot [crown]}$$

$$K_{crown:K^+}^{eq} = \frac{[crown:K^+]}{[K^+] \cdot [crown]}$$

$$K_{sp(BaSO_4)} = [Ba^{2+}] \cdot [SO_4^{2-}]$$

Where K_{sp} is the solubility constant of BaSO₄. Combining these equations, and considering the initial concentration of K₂SO₄ in the target droplets (25mM), we can estimate the ratio between of Ba²⁺ and K⁺ complexes as:

$$\frac{[crown:Ba^{2+}]}{[crown:K^+]} = \frac{K_{crown:Ba^{2+}}^{eq}}{K_{crown:K^+}^{eq}} \cdot \frac{K_{sp(BaSO_4)}}{[SO_4^{2-}]_0 \cdot [K^+]_0} = 6 \cdot 10^{-6}$$

This value suggests that, when the shuttle GNPs loaded with Ba²⁺ encounter the target droplet rich in K₂SO₄, cation exchange occurs, and BaSO₄ precipitation is considerably favoured. Also, under these conditions, the ratio of crown:K⁺ complex to free ligand can be estimated as:

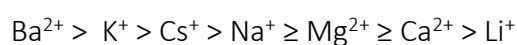
$$\frac{[crown:K^+]}{[crown]} = [K^+]_0 \cdot K_{crown:K^+}^{eq} = 5.3$$

In this case, complexation is initially favoured, with over 84% of the ligand molecules coordinated to K⁺ ions at the starting concentration. However, if the concentration of K⁺ eventually decreases by one order of magnitude as the result of diffusion of shuttle GNPs carrying K⁺, the complexation of K⁺ is drastically impaired (below 35% for 5 mM of K⁺). This suggest that the transport mechanism is not dependent on reverse transport of cations from *target* to *source* droplets by complexation.

Complexation Equilibrium in the Presence of Different Cations.

We have also performed experiments with different sulfate salts within the target droplets, to evaluate the role of cation complexation on the back transport of ions, from the target emulsion towards the source emulsion. If Ba^{2+} ions exchange with other, strongly complexing cations, co-transport of associated SO_4^{2-} ions towards the source droplets could occur and lead to the precipitation of BaSO_4 also in the source droplets, which is never observed.

The complexation data presented in Table ESI1 allow us to establish the ranking of 18C6 coordination affinity for the cations as:



Here we have included Ca^{2+} and Na^+ for comparison purposes, since data for 18C6: Mg^{2+} complexation are not available. Using the stability constants for these complexes, we can estimate that the fraction of 18-crown-6 ligands complexing metal cations within the target droplets falls below 32% for Cs^+ and Mg^{2+} , and drops even lower for Li^+ ($\approx 0.5\%$ of 18C6: Li^+ complexes), which are significantly lower than the predicted values for K^+ (84% for initial K^+ concentration 25mM). We would expect that this drastic change on the ability of cations to interact with the ligand might have a considerable impact on the back transport of the shuttle GNPs, if electroneutrality is maintained when crossing the water/non-ionic-surfactant/chloroform interface. Surprisingly, the results suggest that substituting K^+ for Li^+ , Cs^+ or Mg^{2+} does not impair the performance of the diffusion-controlled system, with formation of BaSO_4 precipitate in the target emulsion for all these metal cation salts (see Figure ESI9). We can therefore conclude, at least qualitatively, that cation complexation within the target droplets is not playing a critical role in the turnover of the Ba^{2+} transport process, and assume that after releasing the cargo within the target droplets, the shuttle NPs can also return “empty” upstream to the source droplets, to continue transporting the Ba^{2+} ions across. This poorer coordination ability of the cations present in the target droplets, alongside depletion of SO_4^{2-} by precipitation of BaSO_4 , will result in a reduced migration of SO_4^{2-} counter ions between the two types of droplets, consistent with the experimental observation of precipitation exclusively within the target droplets.

Estimation of Surface Charge on Shuttle GNPs

We have also investigated the surface charge of the GNPs functionalised with *18-crown-6* in the absence and in the presence of different salts containing coordinating cations. The Z potential of the different systems were measured experimentally, and the apparent surface charge was calculated following Oshima's approximation for salt-free^[8] and general electrolyte solutions.^[9] This model assumes that the electric potential at a distance r from the centre of a spherical nanoparticle obeys a Poisson-Boltzmann equation:

$$\frac{\partial^2 y}{\partial r^2} + \frac{2\partial y}{r\partial r} = - \frac{\kappa^2 \sum_i z_i n_i e^{-z_i y}}{\sum_i z_i^2 n_i}$$

Where y is the reduced electric potential associated to the electric potential $\psi(r)$ and it is

$$\text{defined as } y = \frac{q_e \psi(r)}{K_B T} ; \text{ with the boundary conditions } \left. \frac{\partial \psi}{\partial r} \right|_{\infty} = \psi(\infty) = 0 .$$

In this expression, K_B is the Boltzmann constant, T is the temperature in Kelvin, q_e is the elementary charge, z_i and n_i are the valence and the concentration of each ionic species present in solution, and κ is the Debye-Hückel parameter of the electrolyte solution. To ensure electroneutrality, the nanoparticle surface with a certain charge density σ_z will be surrounded by counter ions of opposite charge (Figure ESI10). A fraction of these counter ions will be strongly bound to the surface, forming a double layer that moves with the particle, while other counter ions will be dissociated into the solution following the Poisson-Boltzmann distribution. The electric potential at the interface between these two regions is experimentally accessible with Z potential measurements (ψ_z), and can be associated with the surface charge density through the Poisson-Boltzmann differential equation above.

Oshima¹¹ proposed an approximate solution of the Poisson-Boltzmann differential equation that leads to the following expression for the surface charge density of a particle (σ_z) dispersed in a general electrolyte solution:

$$\sigma_z = \frac{\epsilon_R \epsilon_0 K_B T}{q_e} \kappa (1 - e^{-y_z}) \left[\frac{2 \sum_i n_i (e^{-z_i y_z} - 1)}{(1 - e^{-y_z})^2 \sum_i z_i^2 n_i} \right]^{1/2}$$

With the reduced surface potential defined as $y_Z = \frac{q_e \psi_Z}{K_B T}$; and $\epsilon_R \epsilon_0$ the electric permittivity of the dispersion media. For the special case of a salt free media, the approximate expression for σ_Z resembles the unscreened Coulomb potential⁹:

$$\sigma_Z = \frac{\epsilon_R \epsilon_0 \psi_s}{a}$$

Using these expressions, we calculated the surface charge density (σ_Z) of the GNPs based on the Z potential values determined experimentally in the presence of different coordinating cations and counter ions associated with local microenvironments at source and target emulsion droplets (Table ESI2). Interestingly, the cation free GNPs display a slightly negative surface charge, that turn into positive values in the presence of Ba^{2+} and K^+ . However, after cation-coordination, σ_Z values are considerably lower than the surface charge densities at the cation coordination layer (σ_C). This may be due to the screening effect of the double layer of counter ions strongly bound to the surface, which reduces the net charge at the interface of the GNPs (Figure ESI10). Combining σ_Z and σ_C values, we have estimated that the extent of charge screening at the double layer (% S_{DL}) is above 86% for all the experimental conditions investigated. This charge screening effect may also facilitate the diffusion of the shuttle GNPs across the water/non-ionic-surfactant/chloroform interface, ensuring electroneutrality of the system.

Note: σ_Z values calculated from zeta potential data using salt-free approximation for the cation-free nanoparticles, and general electrolyte approximation for all other conditions. σ_C where calculated considering complexation equilibrium constants in Table ESI1.

Aqueous media	Cation	IS (M)	ψ_Z (mV)	σ_Z ($q_e \text{ nm}^{-2}$)	σ_C ($q_e \text{ nm}^{-2}$)	% S_{DL}
no salt	-	~ 0	-8.1	$-1.59 \cdot 10^{-3}$	-	-
0.5mM BaCl_2	Ba^{2+}	$1.5 \cdot 10^{-3}$	+25.3	$+1.28 \cdot 10^{-2}$	+3.14	99.6
0.5mM K_2SO_4	K^+	$1.5 \cdot 10^{-3}$	+18.0	$+1.17 \cdot 10^{-2}$	+0.19	86.5
1.0mM KCl	K^+	$1.0 \cdot 10^{-3}$	+19.3	$+8.80 \cdot 10^{-3}$	+0.19	89.8
0.5mM BaCl_2 + 1mM $\text{K}_4\text{Fe}(\text{CN})_6$	$\text{Ba}^{2+}, \text{K}^+$	$1.1 \cdot 10^{-2}$	+2.6	$+5.48 \cdot 10^{-3}$	+3.05	99.8
1.0mM KCl + 1mM	K^+	$1.1 \cdot 10^{-2}$	-24.4	$-4.20 \cdot 10^{-2}$	+0.70	106.1

Table ESI2 Experimental zeta potential (ψ_z), surface charge density (σ_z), surface charge density at the coordination layer (σ_c), and extent of charge screening at the double layer ($\%S_{DL}$) for different experimental conditions associated with source and target micro-emulsion.

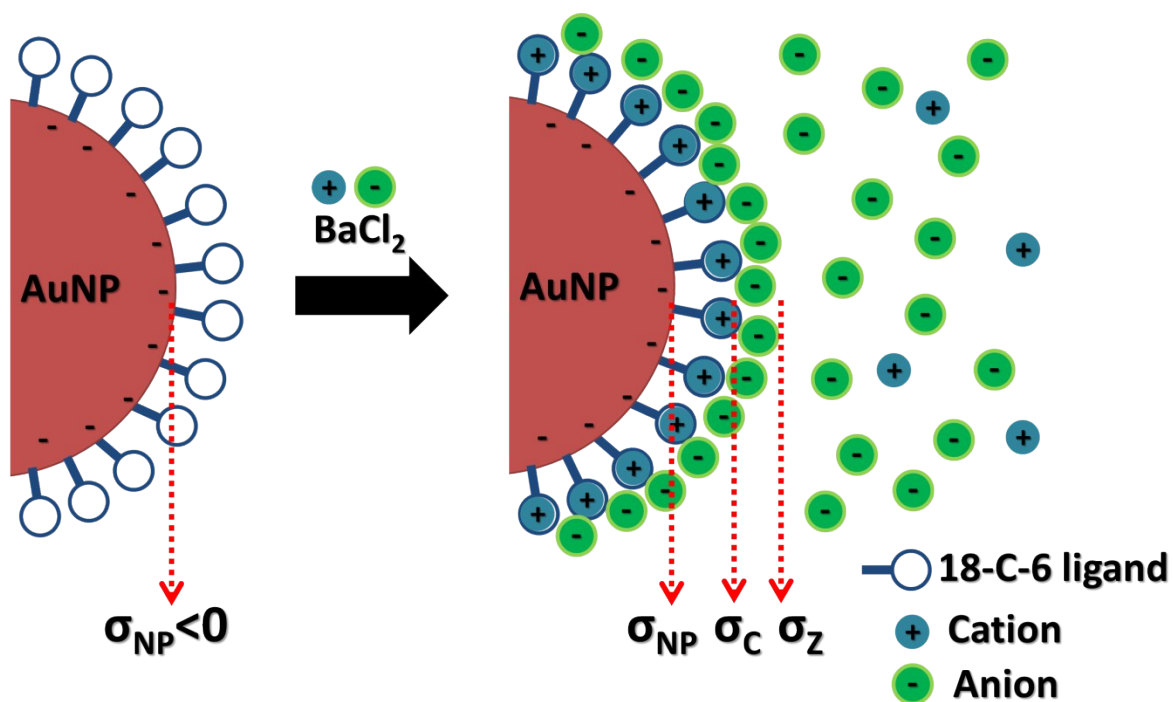


Figure ESI10 Schematic representation of the surface charge density at the different interface layers on the GNPs. Upon coordination of the metal cations, a strongly bound double layer of counter ions screens the charge density at the interface, while other counter ions will be dissociated into solution, following the Poisson-Boltzmann distribution. The extent of charge screening will depend on the balance between counter ion dissociation and double layer binding. σ_{NP} , σ_c , and σ_z are the surface charge densities at the nanoparticle core, at the coordination layer and the double layer, respectively.

5. GNP Phase Transfer

To study the phase transfer behaviour of the larger (7 nm) 18-Crown-6-functionalised GNPs, a simple two-phase experiment was set up. BaCl_2 (1 mM) was added to 5 ml of an aqueous GNP solution (166 nM). Then, 5 ml of chloroform was added creating a simple two-phase liquid/liquid system with the chloroform phase at the bottom. The samples were left to stand and photographed regularly over a six hour period (see Figure ESI11). In the presence of BaCl_2 the GNPs partitioned between the two phases and also accumulated at the interface. In the absence of complexing cations no partitioning was observed.

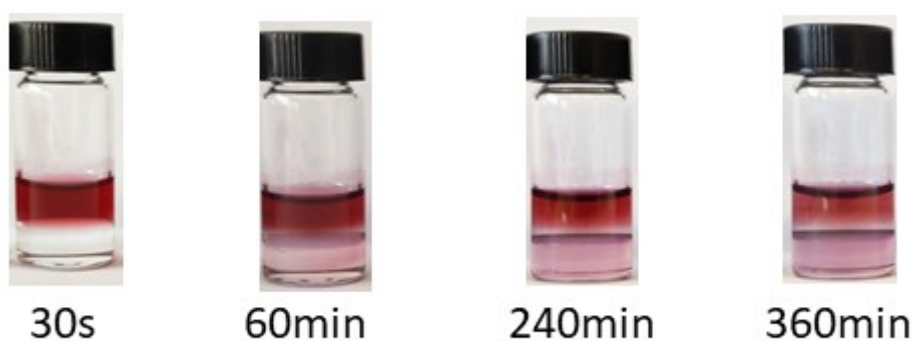


Figure ESI11: Phase-transfer in the presence of BaCl_2 (1 mM) over a 6 hour period, showing the gradual partitioning of GNPs between the aqueous (top) and the chloroform layer (bottom) and some accumulation at the interface.

6. Cryo-SEM

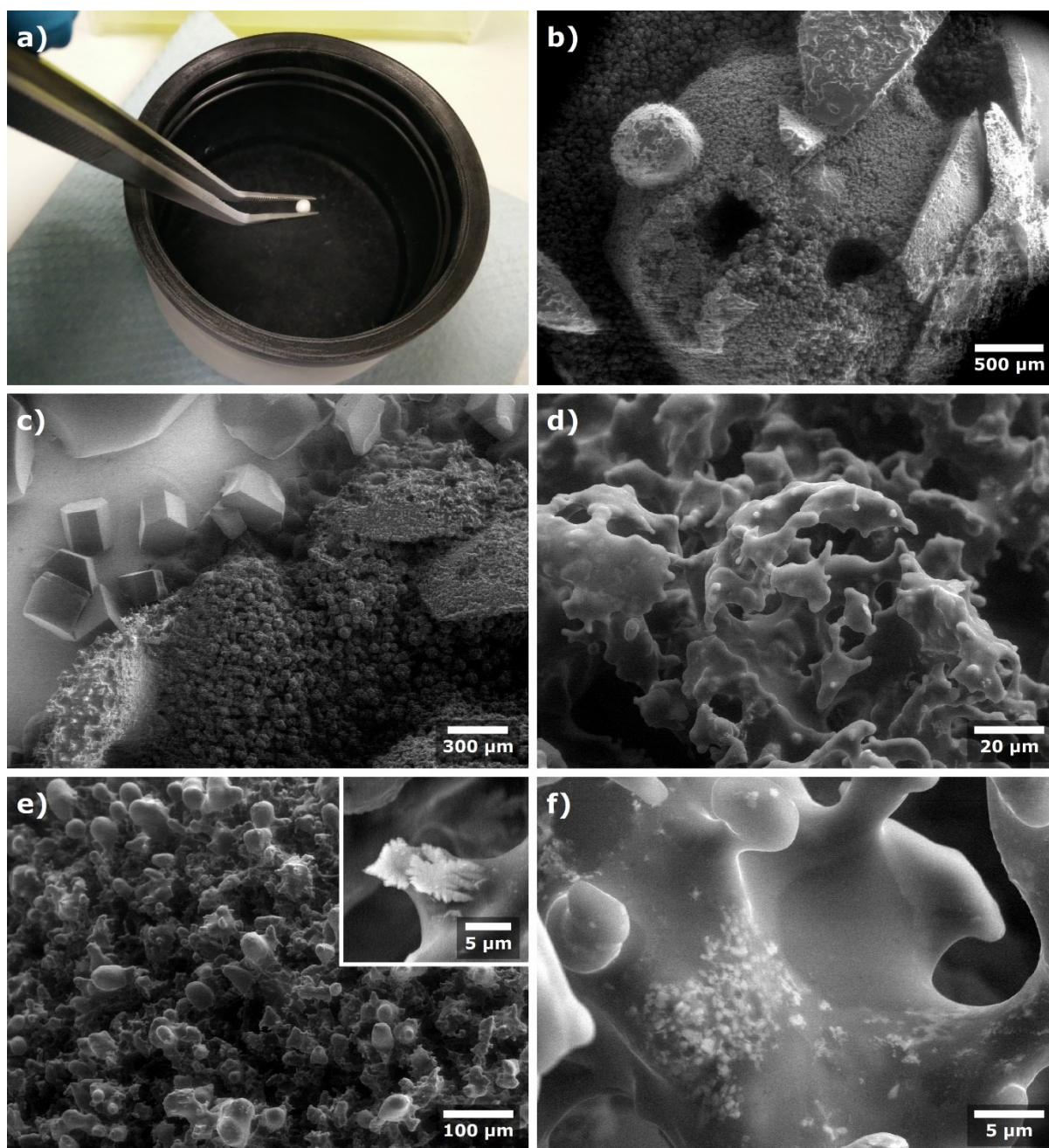


Figure ESI12 Cryo-ESEM images (b-f), showing the sample frozen solid in liquid nitrogen (a) and afterwards crushed using a tweezer (b). Effects of too high humidity in the sample chamber (c) causing ice crystal formation, and too low (d) causing sublimation of the aqueous droplets. Intact frozen droplets are shown in (e) while the inset and (f) show BaSO₄ precipitates from inside a partially sublimed droplet.

7. Movie of BaSO₄ Precipitation

A movie showing the formation of precipitates in the *target* droplets is attached digitally as Supplementary Information. The *target* droplets are clearly distinguished by the presence of the calcein dye giving them a bluish appearance. In this experiment, the *target* droplets contained MgSO₄ (25 mM), and the *source* droplets BaCl₂ (25 mM) and the GNP transporters (166 nM).

The movie is 20 times faster than real time and was obtained under an optical microscope at 20 fold magnification. No coalescence of droplets is observed over its duration, which is further supported by the stable droplet size distribution (Figure ESI13).

The apparent flickering and change in light is due to manual refocusing during data acquisition in order to make sure that some precipitates forming within the 3D droplets remain in focus. This also accounts for the apparent change in droplet size.

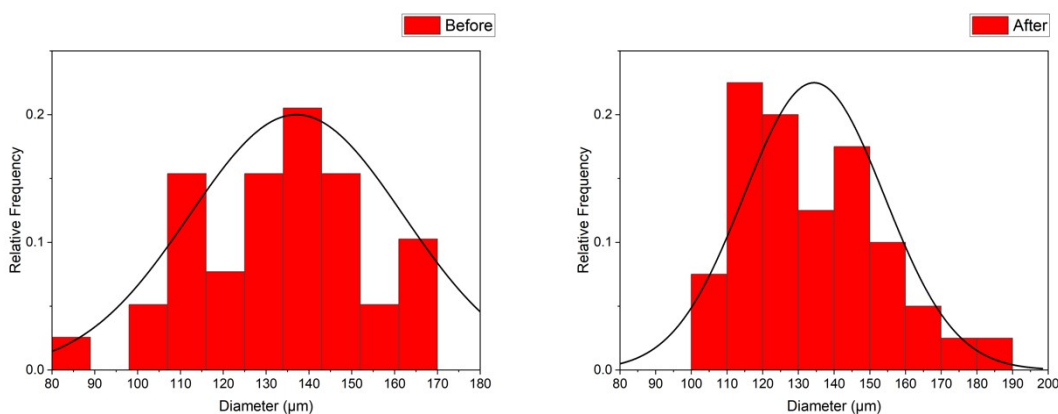


Figure ESI13 Size distribution of droplets before and after acquisition of the movie.

References

- [1] Capdevila, M., Maestro, A., Porras, M., & Gutiérrez, J. M. (2010). Preparation of Span 80/oil/water highly concentrated emulsions: Influence of composition and formation variables and scale-up. *Journal of Colloid and Interface Science*, 345(1), 27
- [2] Griffin, William C. (1949), Classification of Surface-Active Agents by 'HLB', *Journal of the Society of Cosmetic Chemists*, 1 (5): 311
- [3] Peltonen L, Hirvonen J, Yliruusi J. The Behavior of Sorbitan Surfactants at the Water-Oil Interface: Straight-Chained Hydrocarbons from Pentane to Dodecane as an Oil Phase. *J Colloid Interface Sci.* **2001**, 240 (1)
- [4] P. Gruner, B. Riechers, B. Semin, J. Lim, A. Johnston, K. Short and J.-C. Baret, Controlling molecular transport in minimal emulsions, *Nat. Commun.*, **2016** 7, 10392
- [5] Y. Chen, A.W. Gani and S.K.Y. Tang, Characterization of sensitivity and specificity in leaky droplet-based assays, *Lab Chip*, **2012**, 12, 5093
- [6] R.M. Izatt, K. Pawlak, J.S. Bradshaw, R.L. Bruening, Thermodynamic and kinetic data for macrocycle interactions with cations and anions, *Chem. Rev.* **1991**, 91, 1721
- [7] R.M. Izatt, J.S. Bradshaw, S.A. Nielsen, J.D. Lamb, J.J. Christensen, D. Sen, Thermodynamic and kinetic data for cation-macrocycle interaction, *Chem. Rev.* **1985**, 85, 271
- [8] H. Oshima, Surface charge density/surface potential relationship for a spherical colloidal particle in a salt-free medium, *J. Colloid. Interf. Sci.* **2002**, 247, 18

[9] H. Oshima, Surface charge density/surface potential relationship for a spherical colloidal particle in a solution of general electrolytes, *J. Colloid. Interf. Sci* **1995**, 171, 525